Journal of Materiomics 10 (2024) 762–769

Contents lists available at ScienceDirect

Journal of Materiomics

journal homepage: www.journals.elsevier.com/journal-of-materiomics/

Research paper

Observing suppressed polarization in flexible ferroelectric negative capacitance field effect transistors

Chuanlai Ren [a, b, 1], Liyufen Dai [a, c, 1], Congbing Tan [b, d], Guangtong Yuan [b, e], Ke Qu [a], Jinbin Wang [c], Xiangli Zhong [c], Mingqiang Huang [a, ***], Jiyan Dai [f], Gaokuo Zhong [a, b, **], Jiangyu Li [a, b, e, *]

[a] Shenzhen Institutes of Advanced Technology, Chinese Academy of Sciences, Shenzhen, 518055, Guangdong, China
[b] Guangdong Provincial Key Laboratory of Functional Oxide Materials and Devices, Southern University of Science and Technology, Shenzhen, 518055, Guangdong, China
[c] School of Materials Science and Engineering, Xiangtan University, Xiangtan, 411105, Hunan, China
[d] School of Physics and Electronics, Hunan University of Science and Technology, Xiangtan, 411201, Hunan, China
[e] Department of Materials Science and Engineering, Southern University of Science and Technology, Shenzhen, 518055, Guangdong, China
[f] Department of Applied Physics, The Hong Kong Polytechnic University, Hong Kong, 999077, China

ARTICLE INFO

Article history:
Received 10 May 2023
Received in revised form
25 August 2023
Accepted 9 September 2023
Available online 14 October 2023

Keywords:
Negative capacitance field-effect transistors
Ferroelectric
Pulse laser deposition
Mica

ABSTRACT

Negative capacitance (NC) has the potential to enable low power microelectronics beyond the fundamental thermionic limit, and it has been theorized that the thermodynamically unstable NC of ferroelectrics can be stabilized by linear dielectric, making negative capacitance ferroelectric field effect transistors (NC-FeFET) possible. Nevertheless, the validity of NC as a physical concept for ferroelectrics remain contentious despite numerous theoretical and experimental investigations, and the intrinsic ferroelectric NC with suppressed polarization has not been demonstrated except locally at vortex core. While NC-FeFET with subthreshold swing (SS) lower than 60 mV/dec limit has been reported, such device characteristics has not been directly connected to suppressed polarization at materials' level, and alternative mechanisms other than NC have also been proposed. Here we demonstrate stable sub-60 mV/dec SS with hysteresis free I–V in NC-FeFET based on $SrTiO_3/Pb(Zr_{0.1}Ti_{0.9})O_3/SrTiO_3$ heterostructure, and observe its suppressed polarization at both macroscopic and microscopic scales. The intrinsic ferroelectric NC thus is experimentally confirmed and directly connected to NC-FeFET performance, and the mica-based device is also highly flexible and robust under cyclic bending as well as extended heating.

1. Introduction

Negative capacitance (NC) has attracted much attention in recent years as it may decrease subthreshold swing (SS) of a field effect transistor (FET) beyond the lower bound of 60 mV/dec [1,2], widely known as Boltzmann tyranny, which imposes a fundamental limit to reducing power consumption in microelectronics [3]. Ferroelectrics have been extensively explored as a promising candidate for possible negative capacitance field effect transistors (NC-FET), and a large body of theoretical analysis as well as experimental studies of NC have been carried out on both ferroelectric materials and devices [4–7]. Landauer first suggested that the capacitance of a ferroelectric can be negative, based on a phenomenological argument, though it is energetically unstable [8]. Salahuddin and Datta rationalized that such a negative capacitance can be stabilized in an overall positive capacitance device [2], which has profound implication for low power microelectronics. Since then, numerous negative capacitance ferroelectric field effect transistors (NC-FeFET) have been reported with SS lower than 60 mV/dec [9–16], utilizing ferroelectric PVDF [10], $BiFeO_3$ [11], $PbZr_{0.52}Ti_{0.48}O_3$ [12], $Hf_{0.5}Zr_{0.5}O_2$ [14] and $CuInP_2S_6$ [15] as the

* Corresponding author. Shenzhen Institutes of Advanced Technology, Chinese Academy of Sciences, Shenzhen, 518055, Guangdong, China.
** Corresponding author. Shenzhen Institutes of Advanced Technology, Chinese Academy of Sciences, Shenzhen 518055, Guangdong, China.
*** Corresponding author. Shenzhen Institutes of Advanced Technology, Chinese Academy of Sciences, Shenzhen 518055, Guangdong, China.
E-mail addresses: mq.huang2@siat.ac.cn (M. Huang), gk.zhong@siat.ac.cn (G. Zhong), lijy@sustech.edu.cn (J. Li).
Peer review under responsibility of The Chinese Ceramic Society.
[1] These authors contributed equally to this work.

https://doi.org/10.1016/j.jmat.2023.09.008

insulating dielectrics. Here, it is important to note the distinction between NC-FeFET and FeFET, as FeFET exhibits *I*–*V* hysteresis due to polarization switching while NC-FeFET is expected to be hysteresis free. Nevertheless, only a minority of NC-FeFETs reported in the literature exhibit hysteresis free *I*–*V* and sub-60 mV/dec SS simultaneously [4], while the exact microscopic origin of apparent NC characteristics remains contentious. For example, it has been proposed that sub-60 mV/dec SS can arises from polarization switching instead of NC, rending hysteresis in *I*–*V* curves despite a SS lower than 60 mV/dec [17,18].

In fact, even the validity of NC as a physical concept for ferroelectrics has been questioned [19], arguing that it misapplies the Landau-Devonshire theory and draws the wrong conclusion [20]. Indeed, three distinct yet closely related phenomena have been credited as NC on materials level, all of which are subjected to different interpretations. The first is when polarization switches from one orientation to another, across the barrier between two corresponding energy wells, temporary NC state is resulted that can be captured by transient measurement [21]. Such transient NC has shed considerable insight into the energy landscape of ferroelectric [21,22], though its technological potential is limited [6]. Furthermore, it has been proposed that in transient measurement, increase in charge with reduction in voltage is also possible *via* inherent positive capacitance of ferroelectric [23] or reverse domain nucleation and propagation in the absence of NC [24]. The second is intrinsic NC stabilized by a dielectric, resulting in local NC in an overall positive capacitance system as originally theorized [2]. Such a scenario is also questioned, however, since ferroelectric tends to form domains to reduce depolarization energy, making the assumption of homogeneous polarization unrealistic [25]. It has even been suggested that such intrinsic NC is not a physical concept for ferroelectrics [19,20]. This has led to the proposal of extrinsic NC arising from domain wall movement within a multi-domain configuration [25], while the technological application of such extrinsic NC face major challenges in switching time and energy dissipation [6,26].

It is evident from the literature survey that for both fundamental science and technological applications, it is critical to experimentally demonstrate suppressed polarization for intrinsic NC, and connect such microscopic mechanism to device performance, *i.e.* NC-FeFET with sub-60 mV/dec SS and hysteresis free *I*–*V* curve. Neither has been reported yet to our best knowledge. The most compelling evidence of NC in a ferroelectric system so far is spatially resolved steady state NC revealed by scanning transmission electron microscopy (STEM), though its polarization is only suppressed locally in the vortex core [27], and it is difficult to connect such atomic-scale polar structure to device performance. In this work, we use $SrTiO_3$/$Pb(Zr_{0.1}Ti_{0.9})O_3$/$SrTiO_3$ (STO/PZT/STO) as a model system and PZT as a control, and observe that the polarization of PZT is suppressed when sandwiched between STO, resulting in NC-FeFET with hysteresis free *I*–*V* curve and sub-60mV/dec SS. In contrast, control sample without stabilizing STO exhibits large spontaneous polarization at material level as well as hysteretic *I*–*V* and large SS in the corresponding FeFET device. We also demonstrate the robust NC-FeFET performance under large bending deformation, extended bending cycles, and high temperature operation up to 180 °C, all enabled by flexible yet robust mica substrate [28,29].

2. Experimental section

Sample Fabrication: The CFO/SRO/STO/PZT/STO/ZnO heterostructure was prepared *via* pulsed laser deposition system (PLD, Pascal Mobile Combi-Laser MBE) using a KrF excimer laser ($\lambda = 248$ nm, Coherent) operated at a laser repetition rate of 10 Hz. CFO buffer layer of ~5.5 nm thickness was first epitaxially grown on freshly cleaved mica substrate at 600 °C and 50 mTorr oxygen pressure. On the buffer layer, the gate electrode SRO was epitaxially grown at 600 °C in an oxygen atmosphere with a pressure of 80 mTorr. On the surface of SRO gate electrodes, the STO/PZT/STO gate stack with thickness of ~3.8 nm, ~285.6 nm and ~3.8 nm was deposited under an oxygen pressure of 200 mTorr at 600 °C. Afterward, ~38.6 nm ZnO thin film was deposited on the STO films at 400 °C in an oxygen atmosphere with a pressure of 8 mTorr. After PLD growth, the heterostructure were cooled down to room temperature at 25 °C/min cooling rates. Finally, the source/drain electrodes (Au) were deposited by sputtering through a shadow mask to form NC-FeFET device. The channel length (L) and width (W) of the fabricated NC-FeFET device were 340 μm and 50 μm, respectively. Same process was used to fabricate Mica/CFO/SRO/PZT/ZnO/Au FeFET device except the deposition of STO layers.

Film and Device Characterization: The crystalline structure of the Mica/CFO/SRO/STO/PZT/STO/ZnO heterostructure was characterized by using XRD (Bruker/AXS D8-ADVANCE X-ray diffractometer). The cross-sectional TEM specimens were lift-out by Focused Ion beam (FIB, Thermal Fisher Helios G4). TEM images were obtained through an aberration-corrected JEM-ARM300F. Microscopic ferroelectricity of Mica/CFO/SRO/STO/PZT/STO and Mica/CFO/SRO/PZT heterostructure was conducted by dual AC resonance tracking PFM (Asylum Research, Cypher-ES). The first and second harmonic responses were respectively excited at ω_0 and $\omega_{0/2}$, while both measured at ω_0. For the measurement of properties, Au electrodes with a diameter of 100 μm were deposited by sputtering through a shadow mask. The *P*–*V* loops were measured using a Radiant Technology Precision Premium II tester (Radiant Technologies, Inc.) at a frequency of 1 kHz. The output and transfer characteristics of the fabricated NC-FET devices and FE-FET devices were measured using a semiconductor parameter analyzer (Agilent Technologies, B1500A). For the bending text, the mold with different bending radii were used to adhere sample on its surface, and the bending performances of sample were tested by semiconductor parameter analyzer.

3. Results and discussion

The typical energy landscape of a ferroelectric is schematically shown in Fig. 1a, wherein two energy wells with opposite spontaneous polarizations are connected by an energy barrier with a local maximum, making the energy profile nonconvex [30]. In the central part of the energy barrier around the local maximum, the dielectric constant is negative since $\frac{\partial^2 U}{\partial P^2} < 0$, corresponding to a NC, though it is energetically unstable. As a result, the ferroelectric usually sits in either of the energy wells and breaks into 180° domains, as schematically shown in Fig. 1b. However, when the ferroelectric is sandwiched between two linear dielectrics of appropriate thickness, the overall energy profile of the resulting heterostructure becomes convex [31], as schematically shown in Fig. 1c, wherein two energy wells collapse into one and the energy barrier disappear. In other words, the central NC region is stabilized with diminished polarization [27], as schematically shown in Fig. 1d. Consequently, both ferroelectric hysteresis and piezoelectric effect diminish at macroscopic scale. We seek to experimentally verify such theoretical expectations, which has not been reported to our best knowledge.

Inspired by the stabilization of NC *via* linear dielectric, a NC-FeFET with a ferroelectric PZT film sandwiched between two ultrathin dielectric STO layers [32] on flexible mica [33–35] substrate is designed, as schematically illustrated in Fig. 2a, wherein $CoFe_2O_4$ (CFO) and $SrRuO_3$ (SRO) serve as buffer layer and gate electrode,

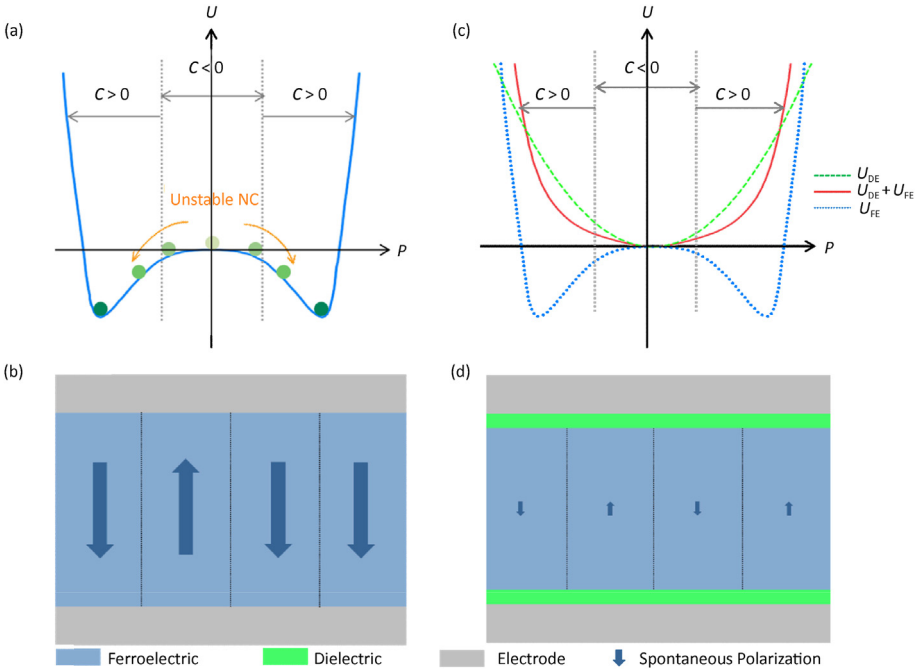

Fig. 1. Phenomenological description of NC. (a) Energy landscape of a ferroelectric, wherein NC around local maxima is unstable. (b) Corresponding structure model of a ferroelectric capacitor. (c) Overall energy landscape of a ferroelectric sandwiched between two thin dielectrics, which stabilize its NC. (d) Corresponding structure model with suppressed polarization in the ferroelectric.

respectively, and ZnO is the semiconducting layer. It is worth noting that in the dielectric-ferroelectric-dielectric structure, the ferroelectric film can works as a quasistatic negative capacitor which is crucial for achieving the hysteresis free *I*–*V* curve [36].The device is fabricated by pulse laser deposition (PLD), as detailed in Experimental Section, and for comparison, the structure without dielectric STO layers is also fabricated. The AFM topography of SRO, PZT and ZnO layers are shown in Supplementary Fig. S1, demonstrating their smooth surfaces, and the crystallinity of heterostructured mica/CFO/SRO/STO/PZT/STO/ZnO is verified by X-ray diffraction (XRD) in Fig. 2b. (*jjj*) reflections from SRO ($j = 2$) and PZT ($j = 1,2$) as well as (00*j*) reflections from ZnO ($j = 2,4$) are observed, indicating the preferential growth along [222]-, [111]-, and [002]-orientation for SRO, PZT, and ZnO, respectively, and the wide-angle XRD

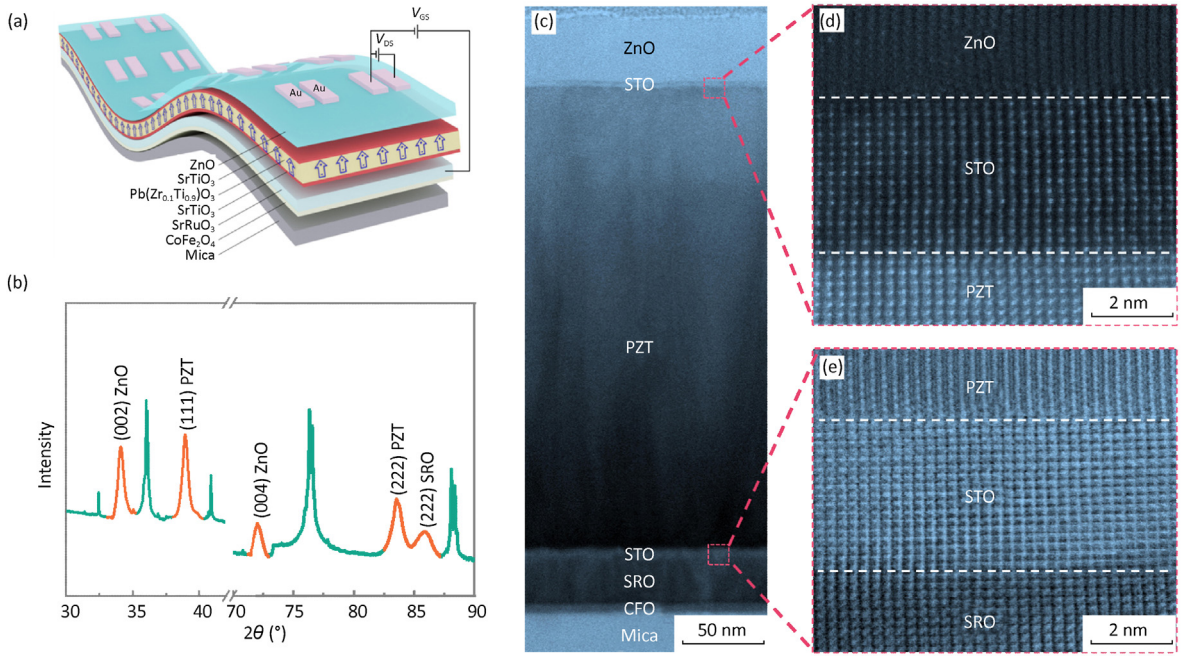

Fig. 2. Configuration and microstructure of flexible NC-FeFET. (a) Schematic configuration of flexible NC-FeFET consisting of mica/CFO/SRO/STO/PZT/STO/ZnO heterostructure with Au source/drain on the top. (b) XRD patterns from mica/CFO/SRO/STO/PZT/STO/ZnO heterostructure. (c) Cross-sectional TEM image of mica/CFO/SRO/STO/PZT/STO/ZnO heterostructure. (d) Zoom-in TEM images from selected regions of PZT/STO/ZnO interfaces. (e) Zoom-in TEM images from selected regions of SRO/STO/PZT interfaces.

patterns in Supplementary Fig. S2 shows no impurity phases. Note that ultrathin STO layer is not detectable *via* XRD, and the corresponding XRD in the absence of STO layers is presented in Supplementary Fig. S3. The high quality CFO/SRO/STO/PZT/STO/ZnO heterostructure is also confirmed by cross-sectional transmission electron microscopy (TEM) in Fig. 2c, revealing clear interfaces between each layer, with the thickness of ZnO, STO, PZT, STO, SRO, CFO and mica estimated to be approximately 38.6, 3.8, 285.6, 3.8, 30.2, 5.5 nm, and 20.0 μm, respectively. Moreover, the energy dispersive X-ray spectroscopy (EDS) element mappings in Supplementary Fig. S4 exhibit uniform distribution of Al, Fe, Ru, Sr, Ti, Pb and Zn in each layer without interfacial diffusion. The higher magnification TEM images in Fig. 2d–e further confirm the sharp and coherent interfaces of PZT/STO/ZnO and SRO/STO/PZT, respectively, while selected-area electron diffraction (SAED) in Supplementary Figs. S5a–b also confirm the single-crystalline ZnO and PZT films. These XRD and TEM data demonstrate the high-quality growth of CFO/SRO/STO/PZT/STO/ZnO heterostructure on mica substrate, and similar high quality is observed in CFO/SRO/PZT/ZnO heterostructure in the absence of STO layers, as shown in Supplementary Fig. S6. Note that the high-quality single crystalline STO/PZT/STO/ZnO heterostructure are critically important for achieving the theoretically expected hysteresis-free NC-FeFET *I*–*V* curve [36,37].

In order to verify that STO dielectric indeed stabilizes the NC of PZT, the characteristics of FeFET based on both PZT and STO/PZT/STO are examined. The output I_{DS}–V_{DS} curves of PZT-based FeFET are shown in Fig. 3a, which is clearly modulated by the gate voltages. The corresponding transfer characteristic under 6 V of V_{DS} is shown in Fig. 3b, exhibiting a counterclockwise hysteresis loop consistent with polarization switching. The SS is determined from the transfer curve as (369.2 ± 18.9) mV/dec, much larger than 60 mV/dec, as expected for the normal behavior of FeFET. The forward transfer curves under different V_{DS} of 6, 5 V and 4 V in Fig. 3c reveal comparable SS of (369.2 ± 18.9) mV/dec, (358.7 ± 21.7) mV/dec and (504.2 ± 28.5) mV/dec consistently larger than 60 mV/dec, and thus no NC is observed in PZT-based FeFET in the absence of dielectric STO. When the two dielectric STO layers each of ~3.8 nm thick is added, however, the FeFET characteristics is changed dramatically. The I_{DS}–V_{DS} output curves in Fig. 3d show similar modulation to Fig. 3a, though the current is reduced due to the increased thickness of the gate stack layer. More interestingly, little hysteresis is seen in the transfer curve under a gate voltage of 3 V, as shown in Fig. 3e, and the corresponding SS is determined to be as small as (23.1 ± 3.7) mV/dec at forward sweeping, much lower than the conventional lower limit of 60 mV/dec, signifying a possible NC. Furthermore, such NC characteristics is very stable under repeated testing, as shown by 5 continuously measured forward transfer curves in Supplementary Fig. S7, which all overlap on each other. We also record the forward transfer curves under different V_{DS} of 1.5, 2.0 V and 3.0 V in Fig. 3f, and the forward transfer curves almost overlap with SS values varying slightly between (19.4 ± 2.1) mV/dec to (22.4 ± 2.4) mV/dec, further confirming the NC of our device is stable. Similarly, when V_{GS} sweeps from −6 V to 6 V in Supplementary Fig. S8, SS value of (31.1 ± 3.4) mV/dec is recorded at forward sweeping. The effect of STO thickness is shown in Supplementary Fig. S9, with SS of (39.1 ± 3.6) mV/dec and (21.0 ± 3.0) mV/dec recorded for 1.9 nm and 3.8 nm STO respectively. Regarding to the reverse sweeping, a traditional subthreshold response rather than NC phenomena was observed from transfer characteristics at both $V_{GS} = \pm 3$ V and $V_{GS} = \pm 6$ V, which may results from the stifled polarization by the emptying/charging of traps in the gate stack heterostructure [38]. Note that the interface density of states (D_{it}) at the ZnO/STO interface is estimated to be about 4.5×10^{12} cm$^{-2}\cdot$eV^{-1}, evaluated based on the expression $SS = \ln(10)\frac{K_B}{q}\left[1+\frac{qD_{it}}{C_G}\right]$ [39], where q is the elementary charge, k_B is Boltzmann constant, T is temperature and C_G is the gate capacitance obtained from capacitance measurements (Supplementary Fig. S10).

In order to understand the mechanism behind the measured sub-60 mV/dec SS, we compare the polarization hysteresis loops of PZT with and without STO layers in Fig. 4a. The Mica/CFO/SRO/PZT/Au capacitor shows robust polarization switching hysteresis, with

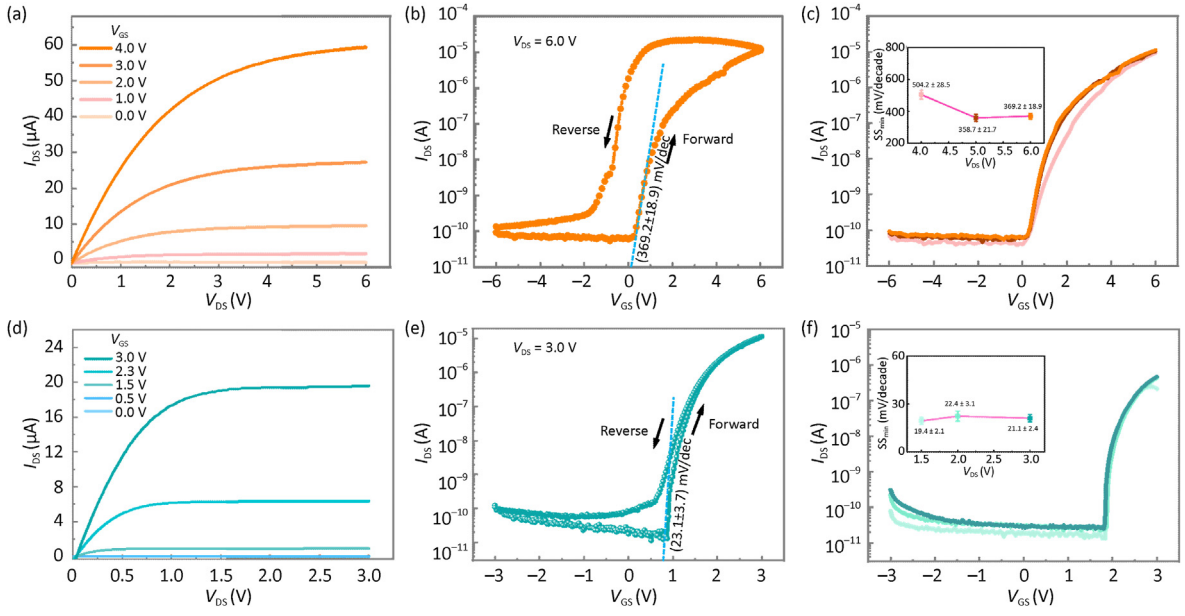

Fig. 3. Electrical characteristics of flexible ferroelectric transistor. (a) Output curves (I_{DS} *vs.* V_{DS}) of the PZT-based FE-FeFET under different gate voltage between 0 and 6 V. (b) Corresponding transfer curves (I_{DS} *vs.* V_{GS}) at V_{DS} = 6.0 V. (c) Forward transfer curves under different V_{DS} of 4.0, 5.0 V and 6.0 V. (d) The output curves (I_{DS} *vs.* V_{DS}) of the STO/PZT/STO-based NC-FeFET under different gate voltage between 0 V and 3 V. (e) Corresponding transfer curves (I_{DS} *vs.* V_{DS}) at V_{DS} = 3.0 V. (f) Forward transfer curves under different V_{DS} of 1.5, 2.0 V and 3.0 V.

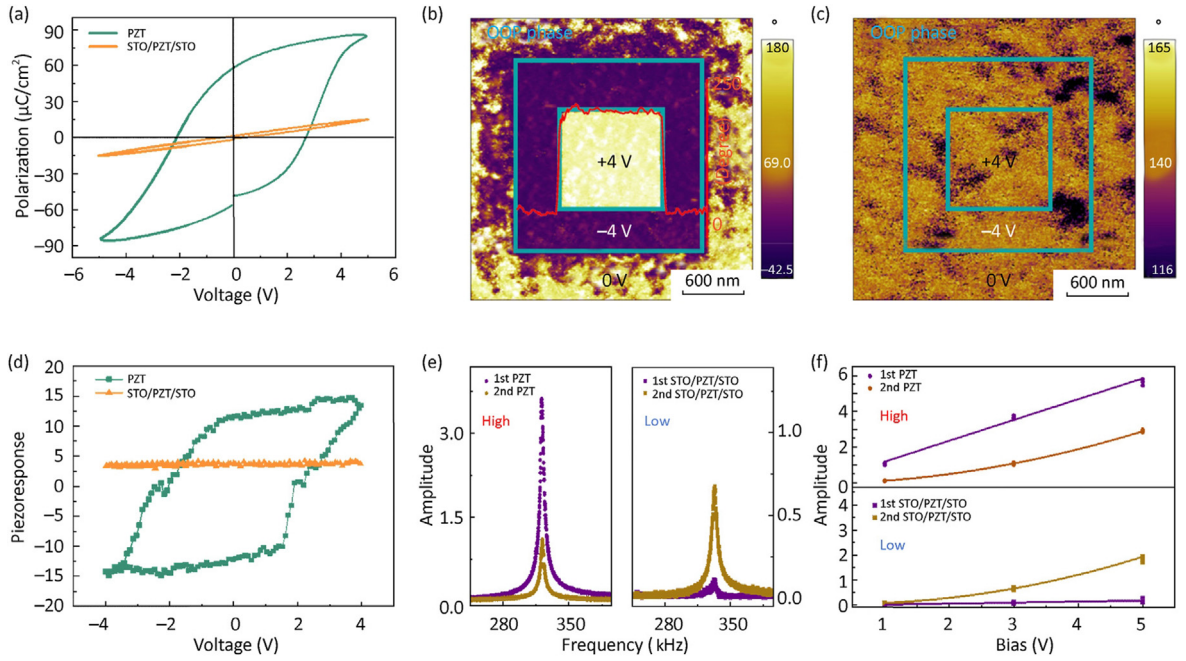

Fig. 4. Ferroelectric characteristics of the PZT and STO/PZT/STO films. (a) *P*–*E* loops of mica/CFO/SRO/PZT/Au capacitor and mica/CFO/SRO/STO/PZT/STO/Au capacitor. (b) Phase mapping of mica/CFO/SRO/PZT after poling. (c) Phase mapping of mica/CFO/SRO/STO/PZT/STO after poling. (d) Piezoresponse hysteresis loops of mica/CFO/SRO/PZT and mica/CFO/SRO/STO/PZT/STO films. (e) First and second harmonic responses of mica/CFO/SRO/PZT and mica/CFO/SRO/STO/PZT/STO films under 3 V AC excitation. (f) First and second harmonic responses of mica/CFO/SRO/PZT and mica/CFO/SRO/STO/PZT/STO films under different AC excitation.

coercive voltage of +2.7 V and −2.1 V and large remnant polarization (P_r) of about 59 μC/cm^2. For the Mica/CFO/SRO/STO/PZT/STO/Au capacitor, on the other hand, PE loop is almost linear with much reduced polarization and diminished hysteresis, suggesting that the polarization is suppressed by the dielectric STO. This contrast has been confirmed by hysteresis loops measured at a series of frequencies, as shown in Fig. S11. We also examine the local ferroelectricity *via* piezoresponse force microscopy (PFM) [40,41], wherein a 1 μm^2 inner box is poled by +4 V DC voltage after the 4 μm^2 outer box is poled by −4 V DC voltage applied through the conductive AFM tip. The poling is successful in PZT, as shown in Fig. 4b, wherein clear 180° contrast corresponding to upward and downward polarizations is observed from PFM phase mapping (the corresponding amplitude mapping in Supplementary Fig. S12. No contrast is seen, however, in STO/PZT/STO shown in Fig. 4c, and the poling fails, consistent with suppressed ferroelectricity demonstrated by Fig. 4a. This can also be verified by point-wise PFM switching in Fig. 4d, with characteristic hysteresis loop for PZT yet linear behavior for STO/PZT/STO. Furthermore the piezoresponse of PZT is dominated by first harmonic response [42–45], as exhibited by both tuning curves in Fig. 4e and variation with respect to AC excitation in Fig. 4f, consistent with built-in spontaneous polarization. STO/PZT/STO, on the other hand, exhibits higher second harmonic response than the first harmonic one, consistent with suppressed polarization. The NC seen at the device level thus is directly connected to suppressed spontaneous polarization at the material level.

To evaluate the reliability of the flexible NC-FeFET, bending tests under different radii and cycles were carried out. As shown in Supplementary Fig. S13, the forward transfer curves remain nearly unchanged under bending radii of 10, 8, 6 mm and 4 mm, with the corresponding SS ranging between (18.7 ± 3.0) mV/dec and (23.9 ± 3.0) mV/dec. Furthermore, after 0, 100, 300 and 500 bending cycles under a small radius of 6 mm as shown in Supplementary Fig. S13b, the forward transfer curves show little variation, with the corresponding SS ranging between (18.0 ± 2.9) mV/dec and (21.9 ± 3.8) mV/dec. One of the defining characteristics of our all-inorganic NC-FeFET is its excellent high temperature capabilities, as shown in Supplementary Fig. S13c, with the forward transfer characteristics curves measured during heating at temperature of 25 °C, 100 °C, 150 °C and 180 °C, exhibiting SS of (22.3 ± 2.6) mV/dec, (25.6 ± 3.7) mV/dec, (28.1 ± 2.9) mV/dec and (34.6 ± 4.0) mV/dec respectively. Furthermore, the forward transfer curves with SS value of (25.3 ± 3.5) mV/dec is recorded after we keep the NC-FeFET at high temperature of 180 °C for an hour, as shown in Supplementary Fig. S13d. These results demonstrate that the flexible NC-FET is robust under high temperature and can be reliably operated over a wide temperature range. For comparison, we summarize the state of art NC-FeFET reported in literature in Supplementary Table 1, and it is evident that our all-inorganic flexible NC-FeFETs not only enjoys a low SS, but also shows robust NC-FeFET performance under large bending deformation, extended bending cycling, and high temperature operation up to 180 °C, which open a route for the application of flexible NC-FeFET.

4. Conclusion

In conclusion, we have explored the relationship between spontaneous polarization, intrinsic NC and device performance of NC-FeFET by using STO/PZT/STO as a model system and PZT as a control, the results suggest that the device performance of NC-FeFET with sub-60 mV/dec SS and hysteresis free *I*–*V* curve can be traced back to the suppressed spontaneous polarization at the material. We also investigated the flexibility and high temperature stability of NC-FeFET, the results indicated that our NC-FeFET not only exhibits remarkable mechanical flexibility with robust operation in bent states having bending radii down to 4 mm and cycling tests of 500 cycles, but also can be operated in a wide temperature range from room temperature to 180 °C. Our work is of significant references for the physical understanding of NC effects and offers a

new option of all-inorganic flexible NC-FeFET for next-generation flexible electronics with low-power consumption and high temperature operation.

Declaration of competing interest

The authors declare that they have no known competing financial interests or personal relationships that could have appeared to influence the work reported in this paper.

Author contributions

The project was conceived and coordinated by JY.L, CL.R and GK.Z. CL.R and LYF.D fabricated the devices and performed the electrical measurements under the guidance of GK.Z and JY.L. The XRD and TEM experiments were carried out and analyzed by K.Q, CB.T, JY.D, CL.R, MQ.H, GT.Y and GK.Z. Ferroelectric and piezoelectric properties were carried out and analyzed by CL.R, LYF.D, GK.Z, MQ.H and JY.L. CB.T, JB.W, XL.Z and GT.Y assisted with data analysis and interpretation. CL.R, GK.Z and JY.L wrote the manuscript, and all the authors participated in discussions and analysis.

Acknowledgments

We acknowledge the support of National Natural Science Foundation of China (12192213, 52302142, 92066203 and 92066102), Shenzhen Science and Technology Program (KQTD20170810160424889, RCYX20200714114733204, JCYJ20200109115219157 and JCYJ20200109115210307), Guangdong Provincial Key Laboratory Program (2021B1212040001) from the Department of Science and Technology of Guangdong Province, Guangdong Basic and Applied Basic Research Foundation (2021A1515110689) and China Postdoctoral Science Foundation (2021M693281). Li also acknowledges Financial Support for Outstanding Talents Training Fund in Shenzhen.

Appendix A. Supplementary data

Supplementary data to this article can be found online at https://doi.org/10.1016/j.jmat.2023.09.008.

References

[1] Ershov M, Liu HC, Li L, Buchanan M, Wasilewski ZR, Jonscher AK. Negative capacitance effect in semiconductor devices. IEEE Trans Electron Dev 1998;45:2196–206.
[2] Salahuddin S, Datta S. Use of negative capacitance to provide voltage amplification for low power nanoscale devices. Nano Lett 2008;8:405–10.
[3] Ionescu AM, Riel H. Tunnel field-effect transistors as energy-efficient electronic switches. Nature 2011;479:329–37.
[4] Alam MA, Si M, Ye PD. A critical review of recent progress on negative capacitance field–effect transistors. Appl Phys Lett 2019;114:090401.
[5] Íñiguez J, Zubko P, Luk'yanchuk I, Andrés C. Ferroelectric negative capacitance. Nat Rev Mater 2019;4:243–56.
[6] Hoffmann M, Slesazeck S, Mikolajick T. Progress and future prospects of negative capacitance electronics: a materials perspective. Apl Mater 2021;9:020902.
[7] Luk'yanchuk I, Razumnaya A, Sene A, Tikhonov Y, Vinokur VM. The ferroelectric field–effect transistor with negative capacitance. npj Comput Mater 2022;8:1–8.
[8] Landauer R. Can capacitance be negative? Collect Phenom 1976;2:167–70.
[9] Salvatore GA, Bouvet D, Ionescu AM. Demonstration of subthrehold swing smaller than 60mV/decade in Fe–FET with P(VDF–TrFE)/SiO_2 gate stack. IEEE Int Electron Devices 2018;2:1–4.
[10] Rusu A, Salvatore GA, Jimenez D, Ionescu AM. Metal–ferroelectric–metal–oxide–semiconductor field effect transistor with sub–60 mV/decade subthreshold swing and internal voltage amplification. Proc IEDM 2010;16:31–4.
[11] Khan AI, Chatterjee K, Duarte JP, Lu ZY, Sachid A, Khandelwal S, et al. Negative capacitance in short–channel FinFETs externally connected to an epitaxial ferroelectric capacitor. IEEE Electron Device Lett 2015;37:111–4.
[12] Dasgupta S, Rajashekhar A, Majumdar K, Agrawal N, Razavieh A, Trolier MS, et al. Sub–kT/q switching in strong inversion in $PbZr_{0.52}Ti_{0.48}O_3$ gated negative capacitance FETs. IEEE J Explor Solid–State Comput Devices Circuits 2015;1:43–8.
[13] McGuire FA, Cheng Z, Price K, Franklin AD. Sub–60 mV/decade switching in 2D negative capacitance field–effect transistors with integrated ferroelectric polymer. Appl Phys Lett 2016;109:093101.
[14] Si MW, Su CJ, Jiang CS, Conrad NJ, Zhou H, Maize KD, et al. Steep–slope hysteresis–free negative capacitance MoS_2 transistors. Nat Nanotechnol 2018;13:24–8.
[15] Wang XW, Yu P, Lei ZD, Zhu C, Cao X, Liu FC, et al. Van der Waals negative capacitance transistors. Nat Commun 2019;10:3037.
[16] Cho HW, Pujar P, Choi M, Kang S, Hong S, Park J, et al. Direct growth of orthorhombic $Hf_{0.5}Zr_{0.5}O_2$ thin films for hysteresis–free MoS_2 negative capacitance field–effect transistors. npj 2D Mater Appl 2021;5:46–53.
[17] Kittl JA, Obradovic B, Reddy D, Rakshit T, Hatcher RM, Rodder MS. On the validity and applicability of models of negative capacitance and implications for MOS applications. Appl Phys Lett 2018;113:042904.
[18] Li XY, Toriumi A. Stepwise internal potential jumps caused by multiple–domain polarization flips in metal/ferroelectric/metal/paraelectric/metal stack. Nat Commun 2020;11:1895.
[19] Van Houdt J, Roussel P. Physical model for the steep subthreshold slope in ferroelectric FETs. IEEE Electron Device Lett 2019;39:877–80.
[20] Liu Z, Bhuiyan MA, Ma TP. A critical examination of 'quasi–static negative capacitance' (QSNC) theory. IEEE Int Elec Dev Meeting 2018;31:1–4.
[21] Khan AI, Chatterjee K, Wang B, Drapcho S, You L, Serrao C, et al. Negative capacitance in a ferroelectric capacitor. Nat Mater 2015;14:182–6.
[22] Hoffmann M, Fengler FP, Herzig M, Mittmann T, Max B, Schroeder U, et al. Unveiling the double–well energy landscape in a ferroelectric layer. Nature 2019;565:464–7.
[23] Saha AK, Datta S, Gupta SK. "Negative capacitance" in resistor–ferroelectric and ferroelectric–dielectric networks: apparent or intrinsic? J Appl Phys 2018;123:105102.
[24] Kim YJ, Park HW, Hyun SD, Kim HJ, Kim KD, Lee YH, et al. Voltage drop in a ferroelectric single layer capacitor by retarded domain nucleation. Nano Lett 2017;17:7796–802.
[25] Zubko P, Wojdeł JC, Hadjimichael M, Fernandez–Pena S, Sené A, Luk'yanchuk I, et al. Negative capacitance in multidomain ferroelectric superlattices. Nature 2016;534:524–8.
[26] Buragohain P, Richter C, Schenk T, Lu H, Mikolajick T, Schroeder U, et al. Nanoscopic studies of domain structure dynamics in ferroelectric La: HfO_2 capacitors. Appl Phys Lett 2018;112:222901.
[27] Yadav AK, Nguyen KX, Hong Z, García–Fernández P, Aguado–Puente P, Nelson CT, et al. Spatially resolved steady–state negative capacitance. Nature 2019;565:468–71.
[28] Chu YH. Van der Waals oxide heteroepitaxy. npj Quantum Mater 2017;2:67–71.
[29] Zhong GK, Li JY. Muscovite mica as a universal platform for flexible electronics. J Materiomics 2020;6:455–7.
[30] Shu YC, Bhattacharya K. Domain patterns and macroscopic properties of ferroelectric materials. Phil Mag B 2001;81:2021–54.
[31] Hoffmann M, Pešić M, Slesazeck S, Schroeder U, Mikolajick T. On the stabilization of ferroelectric negative capacitance in nanoscale devices. Nanoscale 2018;10:10891–9.
[32] Islam Khan A, Bhowmik D, Yu P, Joo Kim S, Pan X, Ramesh R, et al. Experimental evidence of ferroelectric negative capacitance in nanoscale heterostructures. Appl Phys Lett 2011;99:113501.
[33] Zhong GK, Zi MF, Ren CL, Xiao Q, Tang MK, Wei LY, et al. Flexible electronic synapse enabled by ferroelectric field effect transistor for robust neuromorphic computing. Appl Phys Lett 2020;117:092903.
[34] Ren CL, Zhong GK, Xiao Q, Tan CB, Feng M, Zhong XL, et al. Highly robust flexible ferroelectric field effect transistors operable at high temperature with low-power consumption. Adv Funct Mater 2020;30:190613.
[35] Jiang J, Bitla Y, Huang CW, Do TH, Liu HJ, Hsieh YH, et al. Flexible ferroelectric element based on van der Waals heteroepitaxy. Sci Adv 2017;3:e1700121.
[36] Park HW, Roh J, Lee YB, Hwang CS. Modeling of negative capacitance in ferroelectric thin films. Adv Mater 2019;31:1805266.
[37] Pintilie L, Boni GA, Chirila CF, Stancu V, Trupina L, Istrate CM, et al. Homogeneous versus inhomogeneous polarization switching in PZT thin films: impact of the structural quality and correlation to the negative capacitance effect. Nanomaterials 2021;11:2124–40.
[38] McGuire FA, Lin YC, Price K, Rayner GB, Khandelwal S, Salahuddin S, et al. Sustained Sub-60 mV/decade switching via the negative capacitance effect in MoS_2 transistors. Nano Lett 2017;17:4801–6.
[39] Huang JK, Wan Y, Shi JJ, Zhang J, Wang ZH, Wang WX, et al. High-κ perovskite membranes as insulators for two-dimensional transistors. Nature 2011;605:262–7.
[40] Li ZW, Wang YJ, Tian G, Li PL, Zhao L, Zhang FY, et al. High-density array of ferroelectric nanodots with robust and reversibly switchable topological domain states. Sci Adv 2017;3:e1700919.
[41] Zhang Y, Parsonnet E, Fernandez A, Griffin SM, Huyan HX, Lin CK, et al. Ferroelectricity in a semiconducting all-inorganic halide perovskite. Sci Adv 2022;8:eabj5881.
[42] Chen QN, Ou Y, Ma FY, Li JY. Mechanisms of electromechanical coupling in strain based scanning probe microscopy. Appl Phys Lett 2014;104:242907.

[43] Zhong G, An F, Bitla Y, Wang JB, Zhong XL, Yu JX, et al. Deterministic, reversible, and nonvolatile low-voltage writing of magnetic domains in epitaxial $BaTiO_3/Fe_3O_4$ heterostructure. ACS Nano 2018;12:9558–67.
[44] Xia GZ, Huang BY, Zhang Y, Zhao XY, Wang C, Jia CM, et al. Nanoscale insights into photovoltaic hysteresis in triple-cation mixed-halide perovskite: resolving the role of polarization and ionic migration. Adv Mater 2019;31:1902870.
[45] Huang BY, Liu ZH, Wu CW, Zhang Y, Zhao JJ, Wang X. Polar or nonpolar? That is not the question for perovskite solar cells. Natl Sci Rev 2021;8:nwab094.

Dr. Chuanlai Ren received his Ph.D. degree in Materials Science and Engineering from Xiangtan University in 2020. Now, he is a research assistant professor in Southern University of Science and Technology. His research interest focuses on ferroelectric materials and flexible electronics.

Liyufen Dai is a Ph.D. candidate in Materials Science and Engineering at Xiangtan University. Her research interest focuses on ferroelectric materials and flexible electronics.

Dr. Congbing Tan received his Ph.D. degree in Materials Science and Engineering from Xiangtan University in 2018. Now, he is an associate professor in Hunan University of Science and Technology. His research interest focuses on the development of multifunctional oxide film materials.

Guangtong Yuan is a Ph.D. candidate in Department of Materials Science and Engineering at Southern University of Science and Technology. His research interest focuses on the growth of thin films and flexible electronics.

Dr. Ke Qu received her Ph.D. degree in Condensed Matter Physics from Lanzhou University in 2018. She joined Shenzhen Institutes of Advanced Technology, Chinese Academy of Sciences, as a postdoctoral, and now she is an associate professor in East China Normal University. Her research focuses on the atomic resolution structure and electronic structure evolution of transition metal oxides in-situ Cs-corrected transmission electron microscopy.

Dr. Jinbin Wang received his Ph.D. degree in Microelectronics and Solid-State Electronics from Shanghai Institute of Technical Physics, Chinese Academy of Sciences. Now, he is a professor in the School of Materials Science and Engineering, Xiangtan University. His research interest focuses on semiconductors and devices.

Dr. Xiangli Zhong received her Ph.D. degree in Materials Physics and Chemistry from Xiangtan University. Now, she is a professor in the School of Materials Science and Engineering, Xiangtan University. Her research interest focuses on ferroelectric thin-film memory and advanced silicon-on-insulator devices.

Dr. Mingqiang Huang received his Ph.D. degree in Huazhong University of Science and Technology in 2018. Now, he is an associate professor in Shenzhen Institutes of Advanced Technology, Chinese Academy of Sciences. His research interest focuses on the integration of new microelectronic information devices and high energy efficiency computing systems.

Dr. Jiyan Dai received his Ph.D. degree in Institute of Metal Research, Chinese Academy of Sciences. Now, he is a professor in the School of Department of Physics, The Hong Kong Polytechnic University. His research interest focuses on functional oxide thin films and devices.

Dr. Gaokuo Zhong received his Ph.D. degree in Materials Science and Engineering from Xiangtan University. Now, he is an associate professor in Shenzhen Institutes of Advanced Technology, Chinese Academy of Sciences. His research interest focuses on the ferroelectric materials, multiferroics and flexible electronics.

Dr. Jiangyu Li received his Ph.D. degree in Mechanical Engineering from University of Colorado. Now, he is a chair professor in the Department of Materials Science and Engineering, Southern University of Science and Technology. His research interest focuses on advanced scanning probe microscopy and its applications in functional materials.